Volume 1 | Number 1 | Jan 2013 | Pages 1–100

Journal of
Materials Chemistry B

Materials for biology and medicine
www.rsc.org/materialsB

ROYAL SOCIETY OF CHEMISTRY

ROYAL SOCIETY OF CHEMISTRY

www.rsc.org/materialsB

Cadmium free near-Infrared AgInS2/ZnS quantum dots have been synthesized and used for imaging the microenvironment of cancer tumours.
54x50mm (300 x 300 DPI)

Journal Name

ARTICLE

A Toolkit for Bioimaging Using Near–Infrared AgInS$_2$/ZnS Quantum Dots

Armen Shamirian,[a] Oliver Appelbe,[b] Qingbei Zhang,[b] Balaji Ganesh,[a] St0ephen J. Kron,[b] and Preston T. Snee[a]

Presented are a set of procedures to produce water–soluble AgInS$_2$/ZnS near–infrared emitting quantum dots for use as biological imaging agents. The known difficulty of producing near–Infrared core/shell materials is resolved by overcoating the AgInS$_2$ cores at a low temperature using highly reactive precursors. Several methods are explored to impart water solubility of the hydrophobic as–prepared materials. Insofar as achieving aqueous dispersion of quantum dots has only limited biological utility, several methods to further functionalize them are examined. *In vivo* studies are conducted using these quantum dots to demonstrate the ability to model delivery of nanoparticles to the tumour microenvironment.

Introduction

Semiconductor quantum dots (QDs, or nanocrystals) have large number of applications, especially for renewable energy,[1] display technology,[2] and biological imaging and sensing.[3, 4] Quantum dots have strong and broad absorption spectra and narrow size–tuneable emission. As a result, QDs of different sizes can be excited by a single wavelength and emit in separate spectral regions to allow for the simultaneous labelling of different species within a biological milieu.[5, 6] Unlike organic fluorescent dyes, quantum dots are highly photostable due to their inorganic composition and surface passivation which allows for long–term imaging.[7-9]

The first use of the now ubiquitous high quality CdSe/ZnS QDs as bioimaging tools was reported in 1998.[10, 11] Since then many types of colloidal quantum dots composed from groups II–VI (CdSe, CdTe) and III–V (InP, InAs) have been synthesized and used for the same purpose.[12] Due to potential toxicity issues for the most well–developed cadmium containing materials, there are concerns for the future application of these dots in clinical trials.[13, 14] An obvious solution is to develop less toxic QDs for biological applications, and significant research has been devoted towards this goal.[15-18] Materials that emit at specific near-infrared windows are of special interest for *in vivo imaging* applications to the ability to image through deeper tissue mass.[19-22] Among such alternatives, ternary I–III–VI quantum dots have gained a lot of attention due to their long PL lifetime and near–infrared

emissions. They have high extinction coefficients and are overall excellent for *in vivo* imaging; furthermore, their long emission lifetimes may be exploited to minimize background from tissue autofluorescence using time-gated imaging.[23-25] As a result, the synthesis of several I–III–VI semiconductor nanocrystals, such as CuInS$_2$,[26-30] CuInSe$_2$,[31, 32] CuInGaSe$_2$,[33] and AgInS$_2$[34-37] have been reported. These studies have revealed that the main challenge in the synthesis of I–III–VI semiconductors nanocrystals is to impart the correct stoichiometric ratio between the three elements by controlling the reactivity of the two cationic precursors.[38] Xie *et al.* balanced the reactivity of the precursors using alkane thiols ligands to control the reaction rates of group IB ions to obtain high quality ternary quantum dots.[38] As a result, they were able to synthesize high quality CuInS$_2$/ZnS with PL quantum yield of 30% over a 500 nm to 950 nm range of emission. Preliminary results on the synthesis of AgInS$_2$ quantum dots were presented using the same synthetic strategy.

Among the I–III–VI semiconductors, AgInS$_2$ quantum dots are interesting materials due to reduced toxicity issues and near–IR band gap that ranges from 1.87 to 1.98 eV, depending on the underlying crystal structure.[39-41] AgInS$_2$ quantum dots are direct band gap semiconductors with broad PL peaks and large Stokes shifts, which could be explained by "donor–acceptor pairs" model proposed by Krustok *et al.*[42] There are two major approaches for synthesis of AgInS$_2$ ternary QDs. Specifically, the thermolysis of various metal–sulphur complexes or the direct reaction of metal cationic and sulphur precursors. Torimoto *et al.* reported a method for the preparation of ZnS–AgInS$_2$ QDs based on pyrolysis of (AgIn)$_x$Zn$_{2(1-x)}$[S$_2$CN(C$_2$H$_5$)$_2$]$_4$, which resulted in QDs with an emission that can be tuned from 540 nm to 720 nm and a maximum quantum yield of 24%.[43] Burda and co–workers synthesized AgInS$_2$ QDs using Xie's method,[38] which is direct reaction of metal precursors with elemental sulphur in the

a. *Department of Chemistry, University of Illinois at Chicago, Chicago, Illinois, 28807, (USA).*
b. *Department of Molecular Genetics and Cell Biology, The University of Chicago, Chicago, Illinois, 60637, (USA).*

presence of dodecanthiol.[44] They studied how the surface and intrinsic trap states contribute to the emission of the dots. Chang *et al.* measured the effect of different variables such as the molar ratios of metal precursors (Ag:In), the concentration of dodecanthiol capping ligands, the reaction temperature, and the ZnS surface passivation on the luminescence properties of $AgInS_2$ QDs.[45] Tang *et al.* reported the diffusion of Zn in the crystal structure of preformed $AgInS_2$ QDs, which can be used as a strategy for tuning the emission wavelength.[46] They blue shifted the emission by increasing the temperature in the process of overcoating with ZnS. Burda and co–workers studied the mechanism of Ag to Zn cation exchange occurring during the shell growth and they characterized the QDs in each step.[47]

The reports on ZnS coated $AgInS_2$ have shown that the addition of a higher bandgap shell results in a significant blue shift in the emission, which removes one of the motivations for synthesizing these materials to begin with. Burda and co-workers[36] tried to resolve this issue via manipulation of temperature and zinc concentration in the synthesis of core/shell of $AgInS_2$/ZnS. While successful, the quantum yield was not as high as reported for other synesthetic methods that result in blue–shifted emission. As such, an efficient synthesis of high quantum yield yet near–IR $AgInS_2$ / ZnS QDs was developed and is reported herein. Furthermore, many known methods for water-solubilizing and functionalizing CdSe/ZnS QDs were examined with $AgInS_2$ / ZnS QDs. This was done as we do not believe it is safe to assume that previous methods can be successfully applied to new materials even if they share the same zinc sulphide surface. However, in the present study, we can demonstrate that both cap exchange and encapsulation render aqueous dispersions of $AgInS_2$ / ZnS QDs. Additional surface modification with PEG and organic dyes are reported, as well as results from *in vitro* and *in vivo* studies.

Results and discussion

Synthesis and Characterization of $AgInS_2$ Cores

$AgInS_2$ QDs have a ternary composition. Unfortunately, this adds difficulty in their synthesis as binary QDs will form if the reactivities of two cationic precursors are not balanced. Concerning $AgInS_2$, silver is generally the more reactive reagent and Ag_2S QDs may be exclusively synthesized upon injection of sulphur. Based on the work of Xie et al., 1–dodecanthiol ligands were employed to suppress the reactivity of Ag^+ while fatty acids were used to control the reactivity of In^{3+}.[38] The metal and ligands were mixed and degased, after which a sulphur solution in dodecylamine was injected. The dots were grown briefly at 120 °C and were stored under ambient conditions for characterization and subsequent overcoating.

Several methods of characterization were employed. The atomic ratio was found to be $Ag_{1.0}In_{1.0}S_{2.1}$ by XPS as shown in Fig. S1 of the supporting information, which is in good agreement with the expected formula. We conjecture that the slightly higher ratio for sulphur is due to bonding of excess
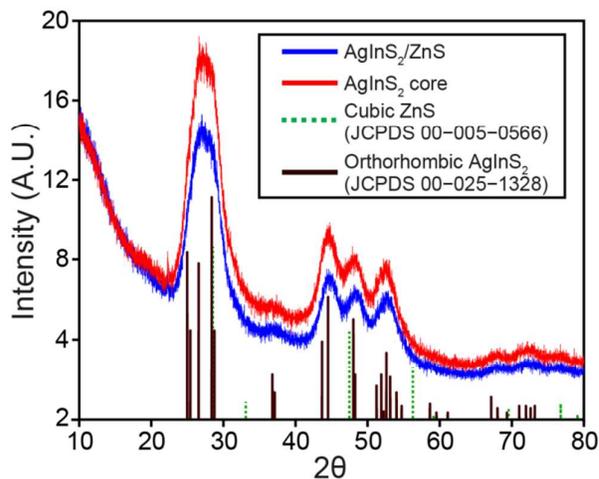

Figure 1. XRD patterns of $AgInS_2$ cores and overcoated $AgInS_2$/ZnS quantum dots.
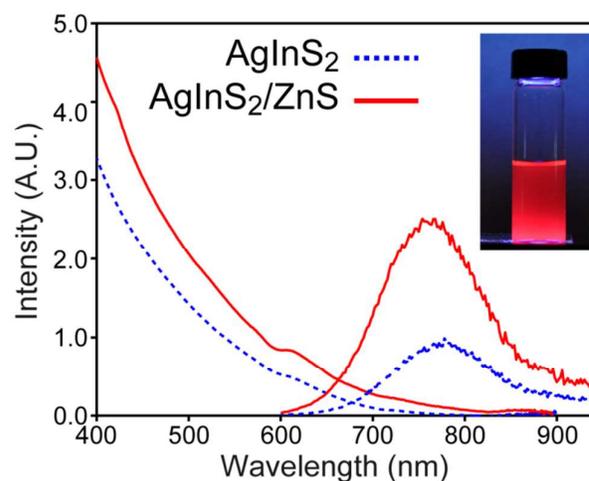

Figure 2. Absorption and emission spectra of core and core/shell QDs. Inset: A photograph of $AgInS_2$/ZnS in hexane under UV excitation. The camera exposure time makes the sample appear brighter than observed visually.

thiol ligands to the surface of QDs. The powder X–ray diffraction shown in Fig. 1 confirms that the sample has a pure orthorhombic crystal structure (JCPDS 00–025–1328). Transmission electron microscopy (TEM) micrographs show that QDs are mostly spherical and single–crystalline particles with size distribution of 3.9 ± 0.8 nm in diameter. The UV–Vis absorption spectrum of $AgInS_2$ cores shown in Fig. 2 does not display excitonic features commonly seen in type II–VI and III–V quantum confined materials. This is generally observed for ternary QDs. The optical band gap of the synthesized $AgInS_2$ cores was calculated to be 1.86 eV by extrapolation of the linear portion of the Tauc plot shown in Fig. S2a. $AgInS_2$ core QDs have broad emission that could not be narrowed by our attempts at size selection. This is likely due to the fact that the broad emission is intrinsic to the material as discussed by Hamanaka *et al.*[48] They proposed that broad emission spectrum is due to donor–acceptor pair recombination as evident from the excitation intensity dependence of the emission spectrum and the observed shift in the time–resolved
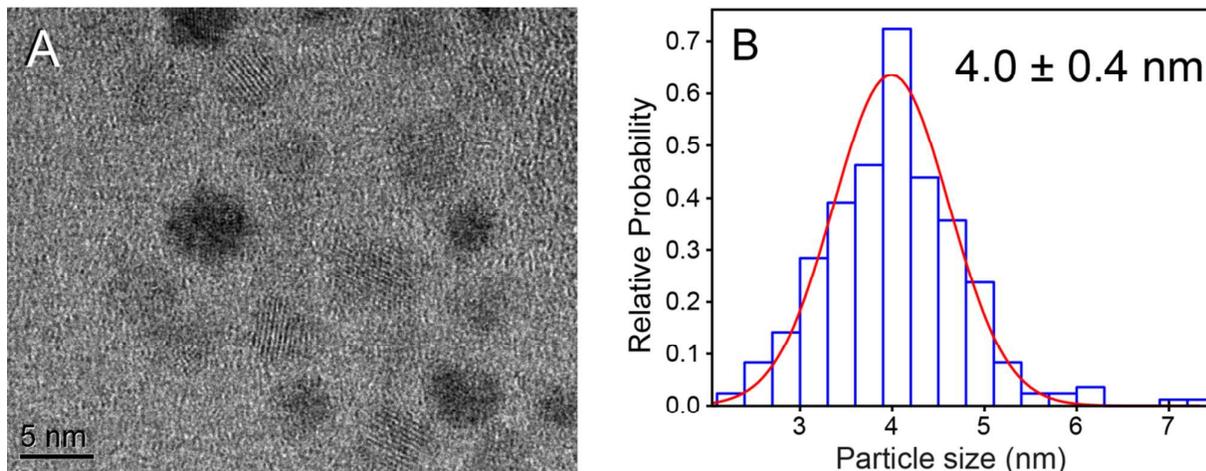
Journal Name

ARTICLE

Figure 3. a) A TEM image of AgInS$_2$/ZnS QDs reveals round, crystalline materials and b) the distribution of particle diameters fitted with a Gaussian function show that the average size is 4.0 ± 0.4 nm.

photoluminescence spectrum. The emission spectrum of the AgInS$_2$ cores followed by a tail off that we attribute to surface defects. As a result, the red tailing portion of the emission spectrum was removed using multiple Gaussian function fitting for quantum yield measurements, see Fig. S3 a,b. Quantum yields of the core AgInS$_2$ quantum dots have been measured using Rhodamine 101 and IRDye®800CW dyes as standards, see Figs. S3c and S3d. Over the course of this study, the range of quantum yield of different batches of core QDs in hexane varied over 4–10%. The core QDs are also highly photostable against continuous irradiation as shown in Fig. S4.

Synthesis and Characterization of AgInS$_2$/ZnS QDs

The challenge with overcoating near–IR emissive AgInS$_2$ cores with zinc sulphide is to prevent the significant blue shift in emission that results from diffusion of Zn from the shell structure into the core and cation exchange of silver by zinc. Tang *et al.* showed that the emission of the AgInS$_2$ QDs can be tuned by incorporation of different amount of zinc at different temperatures.[46] Burda and co-workers studied the partial Ag– to Zn cation exchange in the AgInS$_2$/ZnS QDs.[47] They showed that the extent of zinc diffusion and consequently blue shift in the emission of the QDs depends on the zinc concentration, temperature, and duration of the overcoating process. Our observations are also consistent with these conclusions in that at overcoating at higher temperatures (>180˚C) results in green emitting (525 nm) materials. Thus, a lower temperature needs to be employed; however, coating a core QD often requires elevated temperatures because of the low solubility of the precursors otherwise. Colvin and co-workers showed that ZnS shell can be generated at low temperature by improving the solubility of reactive precursors.[49] They

successfully overcoated CdSe QDs by ZnS at temperature range of 65–180˚C. We modified Colvin's method for overcoating AgInS$_2$ QDs at 140˚C using a n-decylamine / sulphur solution and a mixture of TOP, TOPO, oleic acid, and zinc acetate. Subsequent characterization demonstrated the success of this procedure. The emission spectrum of overcoated QDs is only slightly blue shifted compared to the core, but remains in the near IR region as shown in Fig. 2. Specifically, the band gap of the overcoated QDs was calculated to be 1.83 eV (see Fig. S2), slightly red-shifted compared to the core. Most telling is the fact that the quantum yield of the QDs improved after overcoating, with a variance of 11–28% for samples produced during this study. XPS analysis shown in Fig. S1 revealed the ratio of atoms in the overcoated QDs to be Ag$_{1.0}$In$_{1.0}$S$_{2.8}$Zn$_{0.2}$. The XRD pattern (see Fig. 1) for overcoated QDs is almost the same as cores likely as the orthorhombic AgInS$_2$ spectrum is very similar to cubic ZnS (JCPDS 00–005–0566). TEM images shown in Fig. 3 reveal that size distribution for overcoated QDs is 4.0 ± 0.4 nm. As this is only slightly larger than the cores, it is possible that zinc diffusion and alloying still occurs in the procedure described here.

Water-solubilization of Quantum Dots

There are two major approaches to water-solubilize QDs. One simple method is to encapsulate the QDs into amphiphilic phospholipid or polymer micelles by mixing them with these surfactants in a common solvent. Encapsulation occurs because of the hydrophobic interaction between the polymer and organic caps of the QDs. This method has several advantages, including water-solubilization of QDs without (or minimal) damage to the original surface ligands. This usually results in a better retention of the photoluminescence

Journal Name

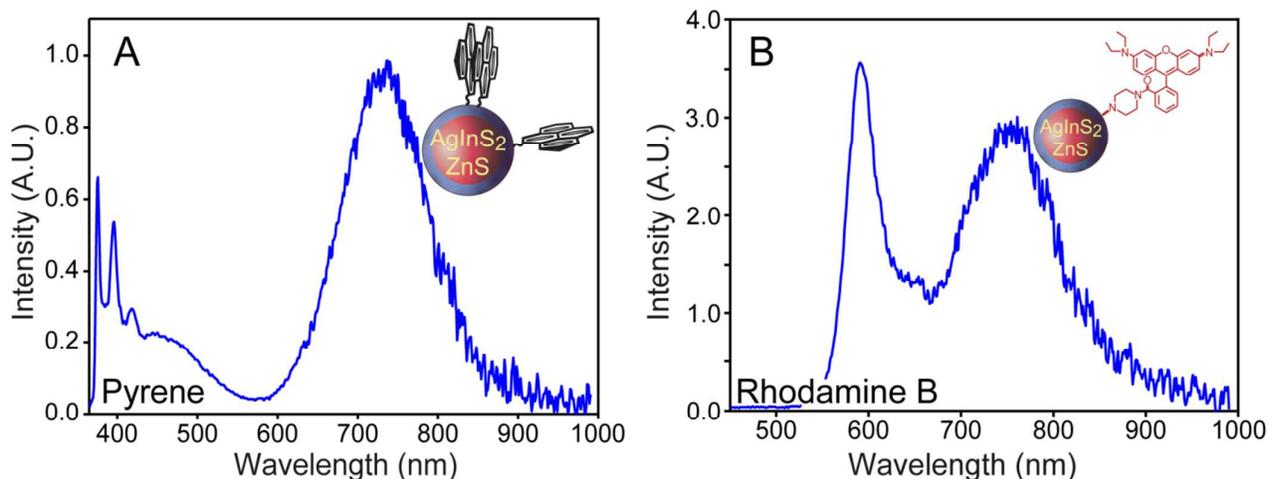## ARTICLE

Figure 4. a) Emission spectrum of pyrene–functionalized polymer-encapsulated AgInS$_2$/ZnS QDs. b) Emission spectrum of Rhodamine B piperazine attached to cap exchanged AgInS$_2$/ZnS QDs. Insets: cartoons of the dot–dye coupled chromophores.

properties after transferring to water. In our experience, the chemical stability in an aqueous environment is such that the dots may stay soluble indefinitely. Last, functionalizing QDs may be enhanced by adding linkable groups to the polymer before coating the nanocrystals. There are different type of modified polymers for encapsulating QDs, and for the purposes of this study, 40% octylamine modified polyacrylic acid was used.[50] It was found that there was no observable loss of materials in the phase transfer process although the quantum yields of the dots decreased by 60% after solubilization. The range of quantum yields of water-soluble QDs has been measured to be 4–10% for polymer encapsulated QDs. Dynamic light scattering (DLS) measurements reveal a ~12 nm hydrodynamic radius as shown in Table S1 of the supporting information; furthermore, at the time of this writing, no materials have been observed to precipitate (~24 months).

Another water-solubilization method is based on ligand exchange on the surface of the QDs, in which the original caps have been replaced by chemical species that impart new solubilities. There are different examples of ligand exchange methods in the literature,[51-53] but many suffer from lack of long term stability and loss of photoluminescence.[54] Recently our group developed a new ligand–exchange method which produces a monolayer of silane coated QDs.[55] These cap exchanged dots can be transferred into water and may remain soluble for ~3 months under ambient conditions. The photoluminescence properties may be comparable and sometimes better than that that observed with polymer-encapsulated QDs. Quantum yields of the water–soluble silane–coated QDs have been measured to 4.5–11%, and they

have a size (~30 nm) comparable to that of polymer-encapsulated dots.

PEGylation of QDs

Water-solubilization is the first step to realize biological applications with QDs. Often imaging studies use QDs coated with polyethylene glycol (PEG) to minimize QD aggregation, enhance salt stability, passivate against protein binding and increase solubility in serum or blood.[56-59] Generally less negatively charged dots are preferred. In this study AgInS$_2$/ZnS QDs were water-solubilized using 40% octylamine–modified polyacrylic acid to make anionic dots as confirmed by gel electrophoresis. Next, they were conjugated PEG 750 amine[60] to the surface of the QDs using a polyethylene glycol carbodiimide crosslinking agent.[61] To investigate the effect of PEG conjugation on the surface charge of the QDs, gel electrophoresis studies were conducted to compare the zeta potential of the QDs before and after conjugation with PEG. The electrophoretic mobility can be calculated by dividing the electrophoretic velocity (migration distance/time) by the electrophoretic potential (voltage applied/gel distance). The zeta potential can be estimated from the electrophoretic mobility using the equation derived by Henry:[62]

$$U = \frac{v \times L}{V}$$

$$\xi = \frac{4\pi\eta U}{\varepsilon}$$

where U is electrophoretic mobility, v is speed of the particle, V is the applied voltage, L is the gel distance, ε is dielectric constant, and η is the viscosity of the medium, and ξ is the zeta potential. As a result, the zeta potential is proportional to the length that the particle travels in a gel. In the present
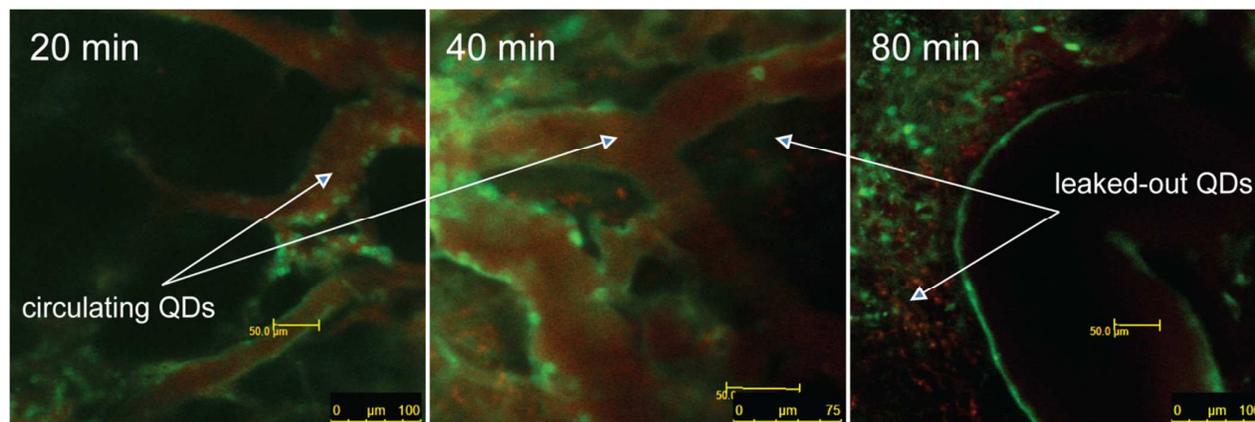
Journal Name

ARTICLE

Figure 5. Quantum dot circulation in microcirculation in BALB-neuT mouse spontaneous mammary tumors at different time intervals.

study, PEGylated QDs migrated less distance compared to the unmodified dots as shown in Fig. S5, which allows us to calculate that the zeta potential of PEGylated QDs is 36.4 % less than non–PEGylated version. Although somewhat indirect, this is evidence of the successful coupling of PEG to the surface of the dots. These materials were used in biological imaging studies as PEGylated polymer-encapsulated QDs have reduced electrostatic charge as demonstrated above and are more stable than silane coated dots. We have also tested the stability in bovine serum after incubation over 24 hours at 35 °C, during which time only a minimal loss materials (~7%) was observed; see Fig. S6 of the supporting information.

Functionalizing QDs

QDs have analytical applications, such as use as nanoscale biosensors, when their photoluminescence properties can be modulated as a response to the presence of a specific analyte.[4] Generally, this ability requires linking the dots to a second, analyte-responsive chromophore, allowing detection via fluorescence resonance energy transfer (FRET), fluorescence intensity modulation or other effects.[63] This requires further surface functionalization of the dots usually with organic dyes as energy transfer–based sensing requires close proximity to the coupled chromophores. There are multiple crosslinking chemistries available that can be exploited to do so, and different types of bonds can be formed as a result.[64] This is generally dependent on the water-solubilization method and the chemical functionalities available in the sensing chromophore. We employed two strategies to create organic dye–water soluble $AgInS_2/ZnS$ QDs coupled chromophores, and to characterize the reaction yields which we were not able to do with the PEGylation experiments. First, polymer-encapsulated water-soluble QDs with carboxylic acid surface caps were conjugated to amine functional organic dyes using

polyethylene glycol carbodiimide. Specifically, a NH_2–PEG–pyrene chromophore and was synthesized and conjugated to 40% octylamine modified polyacrylic acid encapsulated $AgInS_2/ZnS$ dots. The reaction yield can be calculated by comparing absorbance spectra before and after dialysis, which was found to be 60% as shown in Fig. S7a. Dual emission from simultaneous direct excitation of the coupled chromophores is observed in Fig. 4a. This system may also function as a ratiometric sensor for oxygen as pyrene–QD complexes are known to be O_2 sensitive.[65] To demonstrate the ability of $AgInS_2/ZnS$ dot-dye coupled chromophores to function as chemical sensors, pH sensitive aminofluorescein was conjugated to water-soluble QDs. Next, the emission of the coupled chromophores was measured as a function of buffer pH as shown in Fig. S8a of the supporting information. The results demonstrate that the emission of the fluorescein-dye system is a function of the solution pH. Furthermore, photoluminescence excitation spectroscopy demonstrates that fluorescein is an energy donor to $AgInS_2/ZnS$ QDs, which is an unusual observation as organic chromophores are usually poor donors to dot acceptors.[66]

As silane–coated water-soluble $AgInS_2/ZnS$ QDs have thiol surface functional groups, the thiol–to–amine crosslinker sulfo–SMCC was used to attach an amine functional dye. We conjugated Rhodamine B piperazine dye[67] to the silane–coated $AgInS_2/ZnS$ QDs a model for this type of the chemistry. A 95% reaction yield was determined from the absorbance spectra before and after dialysis as seen in Fig. S7b. Dual emission is also observed in this coupled chromophore (see Fig. 4b), which may be further functionalized to create quantum–dot based protein sensors as recently demonstrated.[68]

Cytotoxicity and *In vivo* Studies

Flow cytometry analysis of the HeLa cells after exposure to quantum dots revealed an increase in the number of cells that were DAPI positive, indicating an increase in the cell deaths. There was however no significant increase in the number of cells undergoing apoptosis as indicated by the Annexin positive or Annexin and DAPI positive populations. The increase in cell death correlated with the increase in QD exposure. However, incubation time did not have a significant effect on the cytotoxicity as evident from the insignificant differences in DAPI positive cells observed from 12 h to 48 h exposure. These data are summarized in Fig. S9 of the supporting information.

To examine the potential capabilities of encapsulated and PEGylated AgInS$_2$/ZnS QDs as tools for *in vivo* imaging, BALB-neuT mice bearing spontaneous mammary tumours were injected with QDs along with fluorescein-conjugated tomato lectin by tail-vein injection, 3 days after irradiation of one mammary gland tumour. Using the tomato lectin to visualize endothelial cells lining the tumour microvasculature, distribution of QD's in the irradiated tumour was monitored at intervals by intravital fluorescence imaging as shown in Fig. 5. QDs were observed flowing freely through tumour blood vessels at 20 min. Within 40 min, QDs could be observed extravasating into the tumour tissue, consistent with a loss of microvascular permeability induced by radiation. By 80 min, fluorescence in the circulating blood decreased, likely reflecting elimination via kidney excretion and/or uptake by the reticuloendothelial system, but fluorescence in the tumour persisted. These data demonstrate the potential of tracking of perfusion and delivery of QDs as reporters of macromolecule/nanoparticle delivery to tumours.

Experimental

Materials

Technical grade 1–octadecene (ODE, 90%), indium acetate (99.99%), silver nitrate (>99.8%), zinc chloride (≥98%), caesium carbonate (99%), (3–mercaptopropyl)trimethoxysilane (95%), oleic acid (90%), dodecylamine (≥98%), sulphur powder (99.98%), trioctylphosphine oxide (TOPO) (90%), and 1–dodecanthiol (≥98%) were purchased from Sigma–Aldrich. Trioctylphosphine (TOP, 97%) was purchased from Strem. Zinc acetate (99%) and n–decylamine (99%) were purchased from Acros. Stearic acid (≥97%) was purchased from Fluka. N-(3-dimethylaminopropyl)-N'-ethylcarbodiimide hydrochloride (EDC) was purchased from Advanced Chemtech. 4–(N–maleimidomethyl)cyclohexane–1–carboxylic acid 3–sulfo–N–hydroxysuccinimide ester sodium salt (Sulfo–SMCC) was purchased from Thermo Scientific–Pierce (≥90%). Oleic acid was purified for all syntheses discussed below using the protocol of ref. 69, see also ref. 70 for a video tutorial. All the other chemicals were used without further purification. 40% octylamine–modified poly(acrylic acid) (PAA) was prepared according to refs. 71 and 72. Methoxypolyethylene glycol 750 amine was prepared according to ref. 73. Methoxypolyethylene glycol 350 carbodiimide (MPEG 350 CD) was prepared according to ref. 61 AminoPEG–pyrene and

aminofluorescein chromophores were prepared according to refs. 74 and 75, 76, respectively. Rhodamine B piperazine was prepared according to ref. 67. Chloroform was dried using activated molecular sieves (3 Å, 3.2 mm pellets) from Sigma–Aldrich.

Synthesis of AgInS$_2$ Nanocrystals

This procedure is adapted from ref. 38. A 3–neck 25 mL glass round–bottom flask was loaded with 0.085 g (0.5 mmol) silver nitrate, 0.146 g (0.5 mmol) indium (III) acetate, 0.5 mL (1.58 mmol) oleic acid, 0.5 g (1.75 mmol) stearic acid, and 10 mL of 1–octadecene. The solution was degassed at 90°C, and then 1.2 mL 1–dodecanthiol was added under N$_2$ flow. The solution was heated to 125°C, after which a small portion of TOP (~ 0.2 mL) was added into the solution. This was found to improve the solubility of the resulting AgInS$_2$ quantum dots. A sulphur precursor was prepared by dissolving 0.048 g (1.5 mmol) of sulphur powder in 1.21 g of dodecylamine and degassing under vacuum. This was swiftly injected into the 3–neck flask while rapidly stirring, which was maintained at ~125 °C for 20 min. Afterward, the heating mantle was removed and the solution was allowed to cool to room temperature. The samples were stored under ambient conditions.

Preparation of Zinc Precursor Solution for ZnS Overcoating

A 0.04 M zinc acetate stock solution was prepared by the procedure of Zhu *et al.*[49] First, 0.0734 g (0.4 mmol) of zinc acetate was mixed with 0.5 g of TOPO, 2 mL of TOP, 0.2 mL of oleic acid, and 8 mL of ODE. This mixture was heated to 225°C to obtain a clear solution, which remained transparent after cooling to room temperature.

Synthesis of AgInS$_2$/ZnS Nanocrystals

Half of a batch of AgInS$_2$ dots prepared as described above were processed by precipitation via the addition of ethanol. The supernatant was discarded and the core QDs were dispersed in hexane. A 4–neck 50 mL glass round–bottom flask was loaded with 5 mL of ODE and 4 mL of TOP. The solution was vacuum degassed at 80 °C and then flushed with N$_2$. The core QDs were added and hexane was subsequently removed under vacuum over the course of 1 h. A sulphur precursor was prepared by dissolving 0.005 g (0.15 mmol) of sulphur powder in 2.8 mL of n–decylamine. This solution was injected to the 4–neck flask and stirred for 30 min while maintaining an 80 °C temperature. The temperature was increased to 140 °C and 1 mL of the zinc precursor solution diluted with 2 mL of ODE added slowly through an addition funnel over the course of ~20 min.

Water-solubilizing Using 40% Octylamine–modified Poly(acrylic acid) Polymer

Excess ethanol was added to 0.5 g of the as–prepared AgInS$_2$/ZnS QDs to induce flocculation. The supernatant was discarded, and the precipitate was dried under vacuum. Next, 30 mg of 40% octylamine–modified PAA was added to the QDs followed by ~3 mL chloroform. The resulting solution was sonicated for several minutes to dissolve the polymer completely. The solvent was removed under vacuum and 0.1 M NaOH was added to disperse the QDs into water. It was

found that the use of a strong basic solution increases the phase transfer yield and rate at which the QDs dissolve into water. The excess amount of polymer was removed by dialysis using Amicon Ultra centrifugal filters (100,000 MWCO) from Millipore. D.I. water was used as the diluent and the solution was dialyzed to neutrality. See ref. 77 for a video tutorial on the polymer-encapsulation method.

Water-solubilizing by Silane Coating

As–prepared $AgInS_2$/ZnS QDs were processed following the same procedure as described above. After drying the precipitated materials, ~2 mL of dichloromethane was added to dissolve the QDs followed by 50 μL (0.27 mmol) of (3–mercaptopropyl)trimethoxysilane, 9 mg (0.067 mmol) of zinc chloride, and 88 mg (0.27 mmol) of caesium carbonate. The mixture was stirred overnight. The next day the insoluble caesium carbonate and other by-products were removed by centrifugation. Hexane was then added to the coloured yet clear supernatant to induce precipitation. The precipitate collected by centrifuge and dried under ambient conditions. Two drops of methanol were added to the dried precipitate, and then 0.1 M aqueous NaOH was added. Although only speculative, we believe that the addition of methanol and base causes the outer layer of silane to condense which in turn results in increased stability of the water-soluble QDs. The sample was stirred overnight which generally resulted in QDs fully dispersed in basic water. The sample was dialyzed and diluted by D.I. water using a dialysis tube (Float–A–Lyzer G2, 100 kD MWCO, from Spectrum Labs) to a neutral state.

PEGylation of Water-solubilized QDs

Approximately 1 mL of polymer–encapsulated water-solubilized $AgInS_2$/ZnS QDs was mixed with 10 mg of MPEG 350 CD and was stirred for 15 min. Next, 15 mg of MPEG 750 amine was dissolved in D.I. water and was subsequently acidified to pH 8 with additional phosphate buffers. This solution was added to the quantum dots, and the subsequent pH was adjusted to ~8 by addition of phosphate buffers. Note the solution should never be allowed to have a pH > 9. The mixture was stirred overnight and the next day the solution was dialyzed to remove excess amount of MPEG 750 amine and MPEG 350 CD using Amicon Ultra centrifugal filters (100,000 MWCO) from Millipore.

Reaction Yield for Functionalizing Water-soluble QDs

As the reaction yield of PEGylation is difficult to determine accurately, $AgInS_2$/ZnS QDs were functionalized with organic dyes to evaluate the efficiency of coupling organic species to their surface. In this endeavour, 10 mg of MPEG 350 CD was added to 1 mL of polymer–encapsulated water-solubilized $AgInS_2$/ZnS QDs and was stirred for 15 min. A solution of an amine functional dye, either pyrene PEG amine or Rhodamine B piperazine, in pH 8 phosphate buffer was prepared and was added to the activated QDs solution. Generally, dye was added until a relatively equal emission was observed from the dye and quantum dot under excitation with a UV light. The pH of the solution was adjusted at 8 and was stirred overnight. The next day the solution was dialyzed using Amicon Ultra centrifugal filters (100,000 MWCO) from Millipore.

It was found that the strategy outlined above did not function with any measurable efficiency when synthesizing $AgInS_2$/ZnS QD-aminofluorescein dye coupled chromophores. In this regard, aminofluorescein was first conjugated to 40% octylamine-modified polyacrylic acid using EDC. Unreacted dye was subsequently removed via precipitation of the polymer. Next, the dye-labelled amphiphilic polymer was used to water-solubilize hydrophobic as-prepared $AgInS_2$/ZnS QDs. Further dialysis removed excess dye-labelled polymer.

Silane–coated $AgInS_2$/ZnS QDs were activated using sulfo–SMCC by dissolving 1 mg of this activator in 0.5 mL of pH 6 phosphate buffer followed by adding 1 mL of silane–coated water-soluble QDs. The pH of the solution was adjusted to 7 by adding 0.1 M NaOH and was stirred for 30 min. Next, the solution was run through desalting column to remove excess sulfo–SMCC. A solution of amine functional dye (e.g. Rhodamine B piperazine)[67] in pH 8 phosphate buffer was added to the activated QDs and was stirred overnight. The next day the solution was dialyzed using a dialysis tube (Float–A–Lyzer G2, 100 kD MWCO, from Spectrum Labs).

Cytotoxicity Studies

To evaluate cytotoxicity caused by QDs, HeLa cells were cultured in the presence or absence of quantum dots. To keep the assay physiologically relevant, we used similar concentration of dots that were used *in vivo* studies discussed below. 25 or 100 μL of QDs in water were added to HeLa cells that were cultured in RPMI containing 10% fetal bovine serum. 4',6-diamidino-2'-phenylindole dihydrochloride (DAPI) was used to stain DNA as an indicator for dead cells. Annexin V-FITC was used to stain for phosphatidylserine which egresses from the cell membrane to the cell surface during apoptosis. Annexin V-FITC was used at a concentration of 5 μL /mL and cells were stained for 15 minutes at room temperature. DAPI was added just prior to the running the samples on the flow cytometer at a concentration of 0.5 μM.

In vivo Studies

BALB-neuT is a transgenic mouse line bearing the rat Her2/neu gene under control of an MMTV promoter[43] that serves as a model for sporadic breast cancer. BALB-neuT mice develop multifocal mammary tumours in all ten mammary glands by 30 weeks of age. For these studies, one tumour-bearing mammary gland was irradiated with 15 Gy X-irradiation three days prior to imaging to enhance vascular permeability. Fluorescein-conjugated tomato lectin was purchased from Vector Laboratories. For imaging studies, mice were anesthetized by inhalation of isoflurane gas or i.p. injection of ketamine (90 mg/kg) and xylazine (10 mg kg^{-1}). A Leica SP5 Tandem Scanner Spectral 2-Photon confocal microscope was used for one photon confocal intravital imaging. Skin flap surgery was used to expose tumour tissue and blood vessels while also avoiding any autofluorescence from the skin. Exposed tumours were placed in a glass–bottom petri dish filled with 1× PBS and the dish was placed on the microscope stage for imaging. Fluorescence was imaged with a 20× objective lens plus digital zoom using the 458 nm excitation laser and differing emission spectrum for fluorescein (500-541

nm) and QDs (680-781 nm). All animal studies were performed in compliance and with the approval of the University of Chicago Institutional Animal Care and Use Committee, ACUP# 70931 and 72354.

Characterization

Optical spectra (absorbance) of the samples were measured using a Varian Cary 300 Bio UV/vis spectrophotometer and photoluminescence spectra were obtained using a custom–designed Fluorolog from HORIBA Jobin–Yvon. Dynamic Light Scattering measurements were performed using a Wyatt Dynapro NanoStar (Wyatt Technology, Santa Barbara, CA, USA) in the University of Chicago Biophysics Core Facility. Transmission electron microscopy (TEM) measurements were obtained using a JEOL JEM–3010 operating at 300 keV. X–ray analyses were performed on D8 Advance ECO Bruker XRD diffractometer using monochromatized Cu Kα (λ=1.54056 A˚) radiation. FisherBiotech™ FB–SB–710 horizontal electrophoresis system with FB300 power supply has been used for gel electrophoresis studies. XPS analyses were performed on a monochromatic Al Kα source instrument (Kratos, Axis 165, England) operating at 12 kV and 10 mA for an X–ray power of 120 W. Spectra were collected with a photoelectron takeoff angle of 90° from the sample surface plane, energy steps of 0.1 eV, and a pass energy of 20 eV for all elements. All spectra were referenced to the C 1s binding energy at 284.8 eV. Cell cytotoxicity was detected using a flow cytometer (Becton Dickinson, NJ, USA) to identify Annexin V positive and or DAPI positive cells.

Conclusions

Near infrared AgInS$_2$ QDs were synthesized by balancing the reactivity of silver and indium using 1–dodecanthiol and oleic acid. Core dots were overcoated with ZnS using precursors which are reactive at lower temperatures. Overcoating the QDs in this way resulted in significantly less blue shift in emission compared to previously reported methods, which is likely due to suppression of zinc diffusion as a result of the lower temperatures employed. A three–fold improvement in quantum yield was observed after overcoating which confirms the passivation of the surface of the QDs. Two water-solubilizing methods were successfully used to transfer the QDs into aqueous solutions. Different functionalizing approaches were demonstrated, and amine–functional dyes were attached to QDs that may act as ratiometric sensors and also stand in as models for protein conjugation. *In vivo* imaging studies were conducted to determine the bioimaging capabilities of these PEGylated dots. They revealed that the photostability of the water-soluble QDs is such that NIR emission is observable over the course of several days. Furthermore, the dots have distinctive behaviour compared to other known imaging agents in terms of their localization within murine models.

We hope that this report will help guide researchers into the use of II–III–V NIR emitting semiconductor quantum dots for biological imaging and chemical sensing purposes. A

method to circumvent the problem with retaining NIR emission in AgInS$_2$/ZnS nanocrystals is presented, as well as their use for biological imaging and possibly chemical sensing. Fortunately, known methods for water-solubilization and functionalization of CdSe/ZnS QDs were found to be effective in the case of AgInS$_2$/ZnS dots. However, one motivation for this study is that it is not wise to assume that previously developed procedures will translate to new systems, especially for nanomaterials.

Acknowledgements

Notes and references

1. C.-H. M. Chuang, P. R. Brown, V. Bulovic and M. G. Bawendi, *Nat. Mater.*, 2014, **13**, 796-801.
2. J. S. Steckel, J. Ho and S. Coe-Sullivan, *Photonics Spectra*, 2014, **48**, 55-61.
3. A. P. Alivisatos, W. Gu and C. Larabell, *Annu. Rev. Biomed. Eng.*, 2005, **7**, 55-76.
4. R. C. Somers, M. G. Bawendi and D. G. Nocera, *Chem. Soc. Rev.*, 2007, **36**, 579-591.
5. W. C. Chan, D. J. Maxwell, X. Gao, R. E. Bailey, M. Han and S. Nie, *Curr. Opin. Biotechnol.*, 2002, **13**, 40-46.
6. J. Tian, L. Zhou, Y. Zhao, Y. Wang, Y. Peng and S. Zhao, *Talanta*, 2012, **92**, 72-77.
7. A. Taylor, K. M. Wilson, P. Murray, D. G. Fernig and R. Levy, *Chem. Soc. Rev.*, 2012, **41**, 2707-2717.
8. Z. Kaul, T. Yaguchi, J. I. Harada, Y. Ikeda, T. Hirano, H. X. Chiura, S. C. Kaul and R. Wadhwa, *Biochem. Cell Biol.*, 2007, **85**, 133-140.
9. J. K. Jaiswal, H. Mattoussi, J. M. Mauro and S. M. Simon, *Nat. Biotechnol.*, 2003, **21**, 47-51.
10. M. Bruchez, Jr., M. Moronne, P. Gin, S. Weiss and A. P. Alivisatos, *Science*, 1998, **281**, 2013-2016.
11. W. C. Chan and S. Nie, *Science*, 1998, **281**, 2016-2018.
12. C. M. Tyrakowski and P. T. Snee, *Phys. Chem. Chem. Phys.*, 2014, **16**, 837-855.
13. R. S. McMahan, V. Lee, W. C. Parks, T. J. Kavanagh and D. L. Eaton, *Methods Mol. Biol.*, 2014, **1199**, 155-163.
14. D. K. Scoville, C. M. Schaupp, F. Baneyx and T. J. Kavanagh, *Methods Mol. Biol.*, 2014, **1199**, 179-190.
15. G. Hong, J. T. Robinson, Y. Zhang, S. Diao, A. L. Antaris, Q. Wang and H. Dai, *Angew. Chem. Int. Edit.*, 2012, **51**, 9818-9821.
16. Y.-P. Gu, R. Cui, Z.-L. Zhang, Z.-X. Xie and D.-W. Pang, *J. Am. Chem. Soc.*, 2012, **134**, 79-82.
17. Y. Nakane, Y. Tsukasaki, T. Sakata, H. Yasuda and T. Jin, *Chem. Commun. (Cambridge, U. K.)*, 2013 **49**, 7584-7586.
18. C. Li, Y. Zhang, M. Wang, Y. Zhang, G. Chen, L. Li, D. Wu and Q. Wang, *Biomaterials*, 2014, **35**, 393–400.

19. K. Welsher, Z. Liu, S. P. Sherlock, R. J. T., Z. Chen, D. Daranciang and H. Dai, *Nat. Nanotechnol.*, 2009, **4**, 773-780.

20. G. Hong, J. C. Lee, J. T. Robinson, U. Raaz, L. Xie, N. Huang, J. P. Cooke and H. Dai, *Nat. Med. (N. Y., NY, U. S.)*, 2012, **18**, 1841–1846.

21. G. Hong, S. Diao, J. Chang, A. L. Antaris, C. Chen, B. Zhang, S. Zhao, D. N. Atochin, P. L. Huang, K. I. Andreasson, C. J. Kuo and H. Dai, *Nat. Photonics*, 2014, **8**, 723–730.

22. D. Ghosh, A. F. Bagley, Y. J. Na, M. J. Birrer, S. N. Bhatia and A. M. Belcher, *Proc. Natl. Acad. Sci. U. S. A.*, 2014, **111**, 13948–13953.

23. L. Li, T. J. Daou, I. Texier, T. T. Kim Chi, N. Q. Liem and P. Reiss, *Chem. Mater.*, 2009, **21**, 2422-2429.

24. T. Pons, E. Pic, N. Lequeux, E. Cassette, L. Bezdetnaya, F. Guillemin, F. Marchal and B. Dubertret, *ACS Nano*, 2010, **4**, 2531-2538.

25. H. Zhong, Z. Bai and B. Zou, *J. Phys. Chem. Lett.*, 2012, **3**, 3167-3175.

26. X. Gao, Z. Liu, Z. Lin and X. Su, *Analyst*, 2014, **139**, 831-836.

27. J. Kolny-Olesiak and H. Weller, *ACS Appl. Mater. Interfaces*, 2013, **5**, 12221-12237.

28. S. Liu, W. Na, S. Pang, F. Shi and X. Su, *Analyst*, 2014, **139**, 3048-3054.

29. E. S. Speranskaya, N. V. Beloglazova, S. Abe, T. Aubert, P. F. Smet, D. Poelman, I. Y. Goryacheva, S. De Saeger and Z. Hens, *Langmuir*, 2014, **30**, 7567-7575.

30. J. Park and S.-W. Kim, *J. Mater. Chem.*, 2011, **21**, 3745-3750.

31. T. Omata, K. Nosel and S. Otsuka-Yao-Matsuo, *J. Nanosci. Nanotechnol.*, 2011, **11**, 4815-4823.

32. E. Cassette, T. Pons, C. Bouet, M. Helle, L. Bezdetnaya, F. Marchal and B. Dubertret, *Chem. Mater.*, 2010, **22**, 6117-6124.

33. J. Tang, S. Hinds, S. O. Kelley and E. H. Sargent, *Chem. Mater.*, 2008, **20**, 6906-6910.

34. L. Liu, R. Hu, W. C. Law, I. Roy, J. Zhu, L. Ye, S. Hu, X. Zhang and K. T. Yong, *Analyst*, 2013, **138**, 6144-6153.

35. M. D. Regulacio, K. Y. Win, S. L. Lo, S.-Y. Zhang, X. Zhang, S. Wang, M.-Y. Han and Y. Zheng, *Nanoscale*, 2013, **5**, 2322-2327.

36. B. Mao, C.-H. Chuang, C. McCleese, J. Zhu and C. Burda, *J. Phys. Chem. C*, 2014, **118**, 13883-13889.

37. T. Ogawa, T. Kuzuya, Y. Hamanaka and K. Sumiyama, *J. Mater. Chem.*, 2010, **20**, 2226-2231.

38. R. Xie, M. Rutherford and X. Peng, *J. Am. Chem. Soc.*, 2009, **131**, 5691-5697.

39. Z. Feng, P. Dai, X. Ma, J. Zhan and Z. Lin, *Appl. Phys. Lett.*, 2010, **96**, -.

40. K. J. Hong, J. W. Jeong, T. S. Jeong, C. J. Youn, W. S. Lee, J. S. Park and D. C. Shin, *J. Phys. Chem. Solids*, 2003, **64**, 1119-1124.

41. J. L. Shay and J. H. Wernick, *Ternary Chalcopyrite Semiconductors: Growth, Electronic Properties and Applications*, New York, 1975.

42. J. Krustok, J. Raudoja, J. H. Schön, M. Yakushev and H. Collan, *Thin Solid Films*, 2000, **361–362**, 406-410.

43. T. Torimoto, T. Adachi, K.-i. Okazaki, M. Sakuraoka, T. Shibayama, B. Ohtani, A. Kudo and S. Kuwabata, *J. Am. Chem. Soc.*, 2007, **129**, 12388-12389.

44. B. Mao, C.-H. Chuang, J. Wang and C. Burda, *J. Phys. Chem. C*, 2011, **115**, 8945-8954.

45. J.-Y. Chang, G.-Q. Wang, C.-Y. Cheng, W.-X. Lin and J.-C. Hsu, *J. Mater. Chem.*, 2012, **22**, 10609-10618.

46. X. Tang, W. B. A. Ho and J. M. Xue, *J. Phys. Chem. C*, 2012, **116**, 9769-9773.

47. B. Mao, C.-H. Chuang, F. Lu, L. Sang, J. Zhu and C. Burda, *J. Phys. Chem. C*, 2012, **117**, 648-656.

48. Y. Hamanaka, T. Ogawa, M. Tsuzuki and T. Kuzuya, *J. Phys. Chem. C*, 2011, **115**, 1786-1792.

49. H. Zhu, A. Prakash, D. N. Benoit, C. J. Jones and V. L. Colvin, *Nanotechnology*, 2010, **21**, 255604.

50. X. Y. Wu, H. J. Liu, J. Q. Liu, K. N. Haley, J. A. Treadway, J. P. Larson, N. F. Ge, F. Peale and M. P. Bruchez, *Nat. Biotechnol.*, 2003, **21**, 41-46.

51. H. Mattoussi, J. M. Mauro, E. R. Goldman, G. P. Anderson, V. C. Sundar, F. V. Mikulec and M. G. Bawendi, *J. Am. Chem. Soc.*, 2000, **122**, 12142-12150.

52. S. J. Clarke, C. A. Hollmann, Z. J. Zhang, D. Suffern, S. E. Bradforth, N. M. Dimitrijevic, W. G. Minarik and J. L. Nadeau, *Nat. Mater.*, 2006, **5**, 409-417.

53. M. V. Kovalenko, M. Scheele and D. V. Talapin, *Science*, 2009, **324**, 1417-1420.

54. J. Aldana, Y. A. Wang and X. G. Peng, *J. Am. Chem. Soc.*, 2001, **123**, 8844-8850.

55. X. Zhang, A. Shamirian, A. M. Jawaid, C. M. Tyrakowski, L. E. Page, O. Chen, A. Isovic, A. Hassan and P. T. Snee, *submitted*, 2014.

56. B. Dubertret, P. Skourides, D. J. Norris, V. Noireaux, A. H. Brivanlou and A. Libchaber, *Science*, 2002, **298**, 1759-1762.

57. T. T. Zhang, J. L. Stilwell, D. Gerion, L. H. Ding, O. Elboudwarej, P. A. Cooke, J. W. Gray, A. P. Alivisatos and F. F. Chen, *Nano Lett.*, 2006, **6**, 800-808.

58. W. W. Yu, E. Chang, J. C. Falkner, J. Zhang, A. M. Al-Somali, C. M. Sayes, J. Johns, R. Drezek and V. L. Colvin, *J. Am. Chem. Soc.*, 2007, **129**, 2871-2879.

59. C.-A. J. Lin, R. A. Sperling, J. K. Li, T.-Y. Yang, P.-Y. Li, M. Zanella, W. H. Chang and W. J. Parak, *Small*, 2008, **4**, 334-341.

60. W. Liu, A. B. Greytak, J. Lee, C. R. Wong, J. Park, L. F. Marshall, W. Jiang, P. N. Curtin, A. Y. Ting, D. G. Nocera, D. Fukumura, R. K. Jain and M. G. Bawendi, *J. Am. Chem. Soc.*, 2010, **132**, 472-483.

61. H. Y. Shen, A. M. Jawaid and P. T. Snee, *ACS Nano*, 2009, **3**, 915-923.

62. D. C. Henry, *Proc. R. Soc. Lon. Ser-A,* 1931, **133**, 106-129.

63. C. M. Tyrakowski and P. T. Snee, *Phys. Chem. Chem. Phys.*, 2014, **16**, 837-855.

64. K. E. Sapsford, W. R. Algar, L. Berti, K. B. Gemmill, B. J. Casey, E. Oh, M. H. Stewart and I. L. Medintz, *Chem. Rev. (Washington, DC, U. S.)*, 2013, **113**, 1904-2074.

65. M. Amelia, A. Lavie-Cambot, N. D. McClenaghan and A. Credi, *Chem. Commun. (Cambridge, U. K.)*, 2011, **47**, 325-327.

66. A. R. Clapp, I. L. Medintz, B. R. Fisher, G. P. Anderson and H. Mattoussi, *J. Am. Chem. Soc.*, 2005, **127**, 1242-1250.

67. T. Nguyen and M. B. Francis, *Org. Lett.*, 2003, **5**, 3245-3248.

68. C. M. Tyrakowski and P. T. Snee, *Anal. Chem.*, 2014, **86**, 2380-2386.

69.   R. L. Arudi, M. W. Sutherland and B. H. J. Bielski, *J. Lipid Res.*, 1983, **24**, 485-488.
70.   https://www.youtube.com/watch?v=1Uh2MCR1eRs.
71.   Y. Chen, R. Thakar and P. T. Snee, *J. Am. Chem. Soc.*, 2008, **130**, 3744-3745.
72.   C. M. Tyrakowski, A. Isovic and P. T. Snee, in *Methods in Molecular Biology*, Humana Press, Springer, Netherlands, 2013, vol. 1025, pp. 29-45.
73.   W. Liu, M. Howarth, A. B. Greytak, Y. Zheng, D. G. Nocera, A. Y. Ting and M. G. Bawendi, *J. Am. Chem. Soc.*, 2008, **130**, 1274-1284.
74.   X. Zhang, D. Liu and P. T. Snee, *submitted*.
75.   M. T. Bogert and R. G. Wright, *J. Am. Chem. Soc.*, 1905, **27**, 1310–1316.
76.   R. M. McKinney, J. T. Spillane and G. W. Pearce, *J. Org. Chem.*, 1962, **27**, 3986–3988.
77.   https://www.youtube.com/watch?v=te_qPwYaiug.